Robot-Enabled Uterus Manipulator for Laparoscopic Hysterectomy With Soft RCM Constraints: Design, Control, and Evaluation

Jiahao Wu, *Student Member, IEEE*, Wei Chen, *Student Member, IEEE*, Dezhao Guo, Gan Ma, *Member, IEEE*, Zerui Wang, Yucheng He, *Member, IEEE*, Fangxun Zhong, *Member, IEEE*, Bo Lu, *Member, IEEE*, Yudong Wang, Tak Hong Cheung, and Yun-Hui Liu, *Fellow, IEEE*

***Abstract*—Laparoscopic hysterectomy is a common minimally invasive gynecologic surgery in which an assistant is required to manipulate the uterus during the procedure according to the verbal commands of the primary surgeon. However, uterus manipulation is a lengthy and laborious task, where human fatigue may lower operating safety. This paper presents a novel robot-enabled uterus manipulation system that provides accurate, tireless, and direct uterus manipulation. The system consists primarily of a 7-DoF robotic arm tailored for uterus manipulation in laparoscopic hysterectomy. The primary surgeon can directly control the robot using a footswitch pedal to move within the constraint of the Remote Center of Motion (RCM) via software and achieve the desired range of pitch and yaw motion. An additional rotational motion around the instrument axis is provided for twisting the uterus to enhance the exposure of the ligaments and peritoneum for resection. In addition, the robot arm consists of 7 compact modular actuators that provide the target payload for holding the uterus while maintaining a small footprint in a constrained operating environment. To facilitate operation, a passive mobile base is provided for supporting and positioning the robot. A 6-D force sensor is equipped that allows the assistant to quickly guide the robot into the work area and move the robot under RCM constraint using an admittance control approach. The uterus manipulation rod can be easily detached from the robot body by a quick pluggable mechanism for preoperative sterilization. A quick pluggable mechanism was proposed for easy separation and mounting of the uterus manipulation rod from the robot body for preoperative sterilization. Experiments were performed to measure the performance of the modular joints, RCM repeatability, and evaluate the feasibility of the robot in the simulated laparoscopic hysterectomy.**

***Index Terms*—Laparoscopic hysterectomy, surgical robot, uterus manipulation.**

Manuscript received 4 February 2022; revised 24 April 2022; accepted 31 May 2022. Date of publication 8 June 2022; date of current version 17 August 2022. This article was recommended for publication by Associate Editor P. Poignet and Editor P. Dario upon evaluation of the reviewers' comments. This work was supported in part by the Research Grants Council (RGC) of Hong Kong under Grant T42-409/18-R and Grant 14202918; in part by the Shenzhen-HK Collaborative Development Zone; in part by the Multi-Scale Medical Robotics Centre, InnoHK; in part by the VC Fund 4930745 of the T Stone Robotics Institute; in part by the Project of the Shanghai Municipal Key Clinical Specialty under Grant shslczdzk06302; in part by the Project of the Science and Technology Commission of Shanghai Municipality under Grant 20550760600; and in part by the Project of the Science and Technology Commission of Shanghai Xuhui District under Grant 2020-018. *(Jiahao Wu and Wei Chen contributed equally to this work.) (Corresponding author: Yun-Hui Liu.)*

Jiahao Wu, Wei Chen, Dezhao Guo, Zerui Wang, Yucheng He, Fangxun Zhong, Bo Lu, and Yun-Hui Liu are with the T Stone Robotics Institute and the Department of Mechanical and Automation Engineering, The Chinese University of Hong Kong, Hong Kong (e-mail: yhliu@mae.cuhk.edu.hk).

Gan Ma is with the Sino-German College of Intelligent Manufacturing, Shenzhen Technology University, Shenzhen 518118, China.

Yudong Wang is with the Department of Obstetrics and Gynecology, International Peace Maternity and Child Health Hospital, School of Medicine, Shanghai Jiao Tong University, Shanghai 200240, China.

Tak Hong Cheung is with the Department of Obstetrics and Gynaecology, Prince of Wales Hospital, The Chinese University of Hong Kong, Hong Kong.

Digital Object Identifier 10.1109/TMRB.2022.3181497

I. Introduction

HYSTERECTOMY is a common gynecological surgery to remove the diseased uterus of a female patient [1]. Laparoscopic hysterectomy is an efficient procedure that uses image feedback from the laparoscope to guide the primary surgeon in removing the patient's diseased uterus. Compared to the abdominal hysterectomy, this procedure requires a smaller incision in the abdomen and can shorten the patient's healing time [2], [3]. Fig. 1 shows the layout and division of labor for the laparoscopic hysterectomy. The primary surgeon operates the instrument to remove the uterus, and an assistant (i.e., assistant 1) is responsible for holding the laparoscope. Another assistant (i.e., assistant 2) needs to manipulate the uterus manipulation rod and adjust the posture of the uterus according to the needs of the primary surgeon [4].

However, manipulating the uterus could be tedious and laborious. According to a study of [5], the duration to operate a laparoscopic hysterectomy with and without robot assistance (da Vinci surgical systems [6]) was 154.63 $\pm$ 36.57 minutes and 185.65 $\pm$ 42.98 minutes. The operating performance of the assistant may decline due to the fatigue caused by prolonged continuous operation. Another problem is that the primary surgeon can only verbally order the assistant to adjust the posture of the uterus. This inefficient communication may lead to unsatisfactory uterus configurations.

Manual uterus manipulators, such as the ALLY Uterine Positioning systems of CooperSurgical, Inc. [7] and the SurgiAssist Uterine positioner of SurgiTool, Inc. [8], have been developed to hold the uterus during a laparoscopic hysterectomy to reduce the burden on the assistant. However, a human assistant is still required to manually manipulate these devices to reposition the uterus. By using robotic uterus manipulators, the primary surgeon can directly and remotely manipulate the uterus, while the responsible assistant is relieved from this

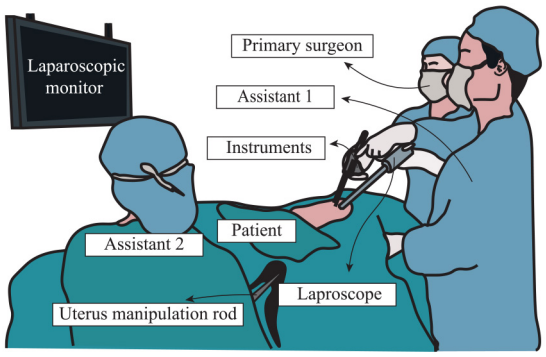

Fig. 1. Basic layout and division of labor during laparoscopic hysterectomy. In this operation, the primary surgeon uses instruments to separate the uterus from the inside of the body. The assistant 1 and assistant 2 are responsible for manipulating the instruments, the laparoscope and the manipulation rod, respectively.

tedious task. And robots can also provide accurate, stable and tireless uterus manipulation [9].

The first robotic uterus manipulator, ViKY Uterine Positioner [10] was developed by EndoControl Medical, Inc. based on the lightweight endoscopic support robot [11], [12]. It consists of a rotation, tilt and insertion mechanism that enables RCM motion through a mechanical approach, but the RCM point can only be located at the vaginal opening and not at the cervix that is anatomically more desirable. Previous studies by Yip *et al.* in our group demonstrated two versions of a three-DoF collaborative robotic uterine positioning system (RUPS) that utilized mechanical RCM motion and had the RCM point located on the cervix [13], [14]. The first version of the robot could only be mounted under a specially modified surgical bed, and the stiffness of the robotic system needed to be improved. The second version has mobile support and uses a novel linearly-actuated arc-guided mechanism to improve mechanical rigidity. However, according to the surgeon's feedback, the pitch range of motion of the robot is still insufficient with the moving range being $-37° \sim 37°$ for certain abnormal conditions, such as hypertrophy and severe adhesion between the uterus and the abdominal cavity. To fully expose the root of the uterus, the desired moving range should be $-50° \sim 34°$. The existing mechanism is unable to achieve a pitch angle of 50° while maintaining a slim robot body. In addition, the assistant needs to use the passive X-Y-Z platform of the robot to adjust the RCM point to the cervix, which prolongs preoperative positioning time.

The implementation of the soft RCM approach provides the robot higher flexibility than the mechanical RCM approach [15], [16]. General serial arm structure is a suitable design for realizing soft RCM, which has a simpler mechanism, slender configuration than the mechanical RCM robots [15], [17]. There are commercially available robotic arms that have been used in minimally invasive laparoscopic surgeries subject to soft RCM constraints, such as the use of the Mitsubishi PA-10 and UR5 (Universal Robots Pte, Denmark) for holding laparoscopic [18], [19], and the LBR iiwa 7 (KUKA, Germany) for manipulating instruments [20], [21]. However, the operating space (located between the patient's legs) for uterus manipulation is far narrower than for the above procedures. The Mitsubishi PA-10 has an approximate height of 1.31 m and a width of 0.25 m, while the Kuka iiwa 7 has a height of roughly 1.27 m and a width of 0.25 m. The space between the patient's legs is a narrow sector, and there is a lot of other medical equipment, so it is difficult for the above robots to get very close to the patient due to the width limitation, and there is a risk of collision with the patient's legs during the movement. The UR5 is smaller than the two robots mentioned above, but its offset joint arrangement still results in a large robot footprint (width 0.25 m) that makes the robot challenging to be placed in the narrow operation space. The UR5 eliminates the Hall sensor and uses a brake with backlash for cost reduction reasons, resulting in slightly wobbled actuation during surgery, which is not conducive to ensuring surgical safety.

This paper proposes a robot-enabled uterus manipulation system (RUM) that is mainly composed of a 7-DOF robotic arm tailored for uterus manipulation in laparoscopic hysterectomy controlled under the constraint of soft RCM that can reach the required pitch motion range $-50° \sim 34°$. To the best of our knowledge, it is the first time a robot complying with soft RCM constraint is used for uterus manipulation targeting laparoscopic hysterectomy. Our robot arm comprises seven high-power-density compact modular actuators, which are mainly integrated with frameless motors, harmonic drives and redundant encoders. Based on the compactness of the modular actuators and the symmetric structure of the robot arm, RUM can hold the uterus while maintaining a small footprint, which is beneficial to introduce this robot into the complex and constraint operation room. The robot's redundant degrees of freedom allow it to achieve a specific end-effector trajectory with minimized joint motions [22]. The distal joint of the robot is coaxial to the rod, which introduces an auxiliary axial rotation for the manipulation rod. According to the suggestion of the collaborated surgeon, through this rotational movement, the robot can twist the uterus to expose more ligaments and peritoneum needed for removal, which was missed in the previous robotics systems. A mobile base is offered to support and position the robot, so there is no need to modify the surgical bed. The quick pluggable mechanism is proposed for easy separation and mounting of the uterus manipulation rod from the robot body for preoperative sterilization. The freely settable joint current, acceleration, and speed limits, which are normally inaccessible in commercially available robot arms, further improve safety. In addition, to facilitate preoperative positioning, the system is equipped with a six-DoF force sensor to let the assistant easily guide the robot to place the RCM point on the cervix by admittance control. The surgeon and assistant can control the robot through footswitch pedal and force sensor handle. As a result, compared to manual uterus manipulation, our system provides more accurate, tireless and direct uterus manipulation based on a customized 7-DOF robotic arm with soft RCM constraints while overcoming the shortcomings of the other robotic uterus manipulation systems.

The rest of the paper is organized as follows: In Section II, we demonstrate the design requirement of the robot-assisted laparoscopic hysterectomy. In Section III, we describe the mechanical structure of the robot-enabled uterus manipulator.

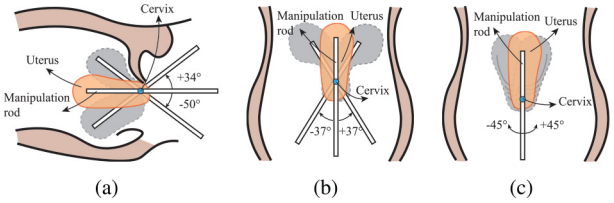

Fig. 2. Motion range of the uterus manipulation rod during laparoscopic hysterectomy. (a) The pitch manipulation (antevetion/retroversion) range is $-50° \sim 34°$; (b) The yaw manipulation (lateral manipulation) range is $-37° \sim 37°$; (c) The roll manipulation (twist) range is $-45° \sim 45°$.

In Section IV, the control strategies of the robot are proposed. In Section V, several experiments are conducted to evaluate the performance of the proposed robotic systems. Conclusions and future works are presented in Section VI.

II. Design Requirements of the RUM

During the laparoscopic hysterectomy surgery, the manipulation rod will be inserted into the patient's uterus to tighten it and adjust its configuration (see Fig. 2). Based on our previous experimental data and the suggestions of our collaborative surgeons, the robot should be developed under the following requirements:

(1) The robot can manipulate the uterus along the required directions (i.e., the lateral motion, the anteversion/retroversion motion) and twist the uterus clockwise/counterclockwise;
(2) The robot should be constrained to move around the cervix, i.e., the RCM point should be located at the cervix;
(3) The preoperative positioning of the robot should be quick and easy;
(4) The robot can be conveniently deployed into existing operation environments.

Specifically, for the first requirement, the robot should meet the range of motion requirements for uterus manipulation (see Fig. 2). Note that the anteversion angle is increased from $-38°$ to $-50°$ as discussed in Section I. For the yaw manipulation range, we set it as before [14], i.e., $-37° \sim 37°$. The roll motion is introduced as a new requirement, allowing the robot to twist the uterus to expose more ligaments and peritoneum that need to be removed, whose motion range is set as $-45° \sim 45°$.

Due to the female anatomic constraints, it is desirable to let the manipulation rod have a remote fixed revolution joint located at the cervix (i.e., RCM feature), which reduces the crushing deformation injury of the manipulation rod on tissues and organs during manipulation. Robot-assisted surgery may require massive preoperative preparation time [23], [24] for the setup of the robot. Especially for the RUPS, the surgeon must adjust the position of the RCM point of the robot by manually tuning the passive X-Y-Z base positioning platform, which is time-consuming and unintuitive. Therefore, it is necessary to provide a quick and convenient preoperational setup approach for robot-assisted surgery. The operating room is very crowded, full of surgeons, assistants and surgical equipment. In addition to this, the space that can be occupied by the robot (only the space between the patient's legs) is very narrow. These reasons lead to strict requirements for the size of the robot and ease of integration.

III. Design of the RUM

To meet the design requirements of the robot mentioned above for uterus manipulation in laparoscopic hysterectomy, the corresponding mechanisms were proposed and developed for each requirement.

A. The Overall Structure of the Robotic System

As shown in Fig. 3(a), the whole system is mainly composed of a passive mobile base and a 7-DoF robot arm. The mobile base can enhance the mobility of the whole system and accommodate electrical components such as industrial computers, power supplies and control boxes of the force sensor. The base is built using stainless steel to increase the weight. Four manually lockable Foma wheels are mounted evenly on the chassis, and they can rotate freely around their own vertical central axis to function as universal wheels.

Serial robot arms can manipulate uterus targeting laparoscopic hysterectomy while maintaining RCM constraints by software. However, conventional industrial serial robot arms and some collaborative robots such as UR5 and LBR iiwa are not well suited for this task directly, as mentioned in Section I. Therefore, we developed a highly customized, 7-DoF robot arm for active uterus manipulation during laparoscopic hysterectomy, which employs a symmetrical design scheme where the joints are unbiased in the horizontal direction. The body of the robot arm is made of aluminum alloy, and its total weight is only 12.02 kg with an estimated rated payload of about 50 N applied to the end-effector frame (see Fig. 5(a)), but the overall size and footprint are smaller than that of the UR5. The UR5 is roughly 1 m in height, but instead has a maximum width of 0.26 m due to the asymmetrical joint layout. Our robot has a height of 0.86 m and a width of 0.15 m, which makes it more compact than UR5. The distal joint of the system (i.e., joint 7) is coaxial to the manipulation rod (see Fig. 3(a) and Fig. 4(b)) that allows decoupled control of the axial rotation of the manipulation rod. This motion is important for the surgery to twist the uterus to expose more ligaments and peritoneum to be removed, which was not available in previous robotic systems. Since the last joint enables direct axial rotation of the instrument, no other joints of the robot arm are required to generate motion. This design reduces the risk of collision between the robot and the patient due to excessive motion of the robot during the procedure. The first six joints of the robotic arm have the same joint arrangement as LBR iiwa, i.e., the rotation axes of joints 1 and 2, joints 3 and 4, and joints 5 and 6 intersect. However, the arrangement of the seventh joint is different from LBR iiwa (see Fig. 4), where the rotation axes of the seventh joint and the sixth joint do not intersect, and the vertical distance between them is d_{offset}. With this layout, it is possible to detached the instrument from the tail of the seventh joint in case of emergency stop of the robot.

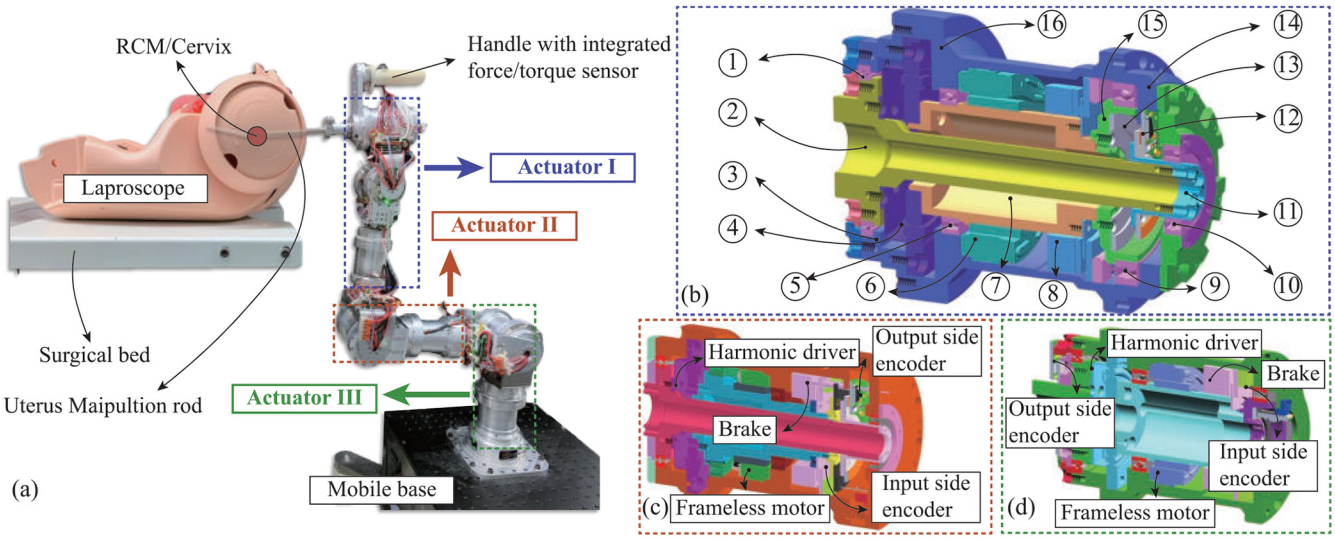

Fig. 3. The whole structure of the robot. (a) The robot-enabled uterus manipulator (RUM) with manikin; (b) Modular actuator III with high output torque; (c) Modular actuator II with medium output torque; (d) Modular actuator I with low output torque.

TABLE I
ESSENTIAL PARTS OF THE ACTUATOR III

1. Cross roller bearing	2. Output shaft	3. Output side bearing support	4. Harmonic driver
5. Motor side bearing	6. Frameless motor	7. Rotor supporting shaft	8. Electromagnetic brake
9. Sensor side bearing	10. Auxiliary bearing	11. Absolute encoder support	12. Absolute encoder
13. Incremental encoder	14. Sensor side bearing support	15. Incremental encoder support	16. Stator supporting shell

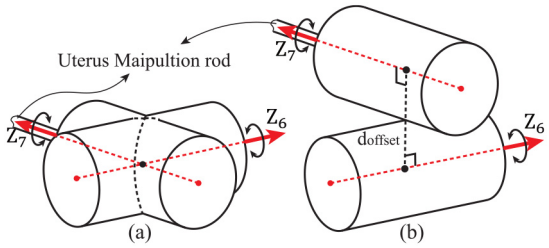

Fig. 4. The comparison of the two types of joint arrangement. (a) The axes of rotation of joints 6 and 7 are perpendicular and intersecting. (b) The axes of rotation of joints 6 and 7 are perpendicular but not intersecting.

TABLE II
PARAMETERS OF THE MODULAR ACTUATOR

Type	Actuator I (Axes 1-2)	Actuator II (Axes 3-4)	Actuator III (Axes 5-7)
Dimensions (mm)	$\phi 102 \times 143$	$\phi 80 \times 133$	$\phi 70 \times 104$
Mass (kg)	2.2	1.7	1.3
Rated Torque (Nm) (after reducer)	100	50	27
Rated Speed (rpm) (after reducer)	26	35	54

B. The Design of the Modular Actuator

Our customized robot arm is formed of compact modular actuators to make the development and integration easy and reliable. As shown in Fig. 3(a), in the order of the output torque from minimum to maximum, the robot is composed of three Actuator I, two Actuator II, and two Actuator III. The detailed inside design of these actuators is shown in Fig. 3(b)-(d).

Take the Actuator III (see Fig. 3(b) and Table I) as an example, it comprises of a high-power-density frameless motor (TQ Group, Germany), a component set harmonic gear reducer (Harmonic Drive Systems, Japan), an incremental encoder (18bt, Renishaw PLC, U.K.), an absolute encoder (19bt, Renishaw PLC, U.K.) and a zero-gap brake (TQ Group, Germany). The high power density frameless motor and component set harmonic gearbox ensure high output torque while maintaining a compact structure of the modular. The actuator has an overall cylindrical shape and has a central through-hole for wire routing. Redundant dual encoders (an incremental encoder to measure motor motion and an absolute encoder to measure output shaft motion) and a gapless brake are used to reduce the risk of motion failure and loss of control of the robot arm. The use of crossed roller bearings improves the stiffness of the joints. Two other types of modular actuators have been developed to meet different torque and volume requirements (see Fig. 3(c)-(d)). Actuator II uses a smaller size motor and harmonic reducer than Actuator III and reverses the motor to help reduce the size of the bearing on the input side and outside. Due to the small size of actuator I, the two encoders were placed on different sides of the joint. Thus the portion of the output shaft through the rotor support shaft in actuator III could be removed to ensure that the diameter of the center hole was large enough for passing the cable and the manipulation rod. The basic parameters of these actuators are shown in Table II. These actuators could provide a large rated

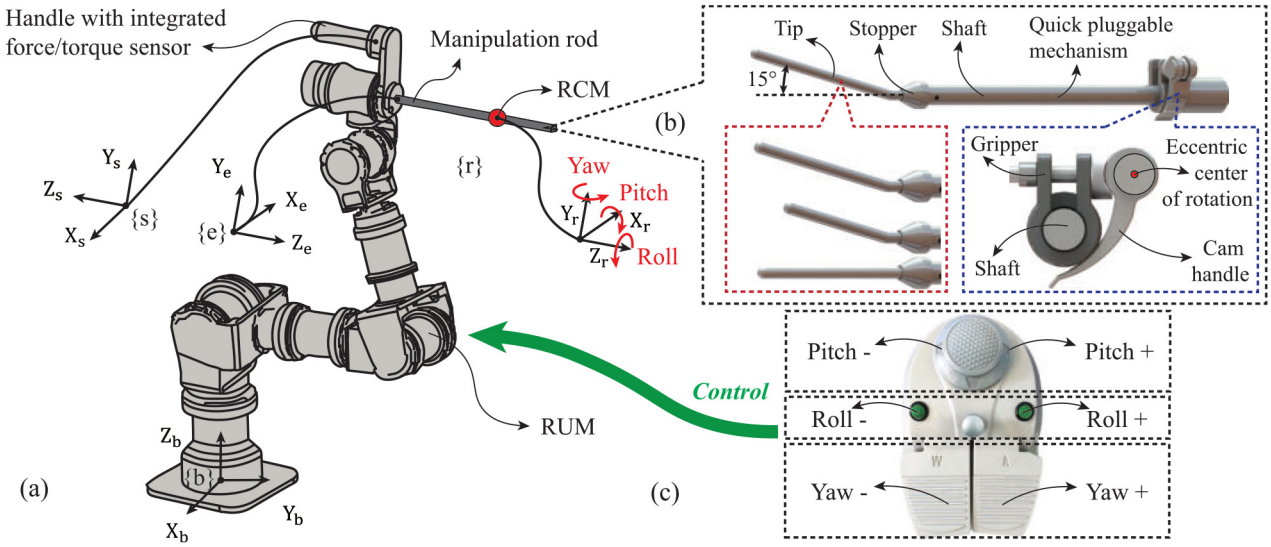

Fig. 5. RCM motion of the RUM. (a) Setting frames and RCM motions for the robot control. (b) The uterus manipulation rod with different rod tip, as well as the quick pluggable mechanism. (c) The foot-pedal interface. The bottom pedals control the yaw motion of the RUM, the medium green buttons control the roll motion, and the top joystick controls the pitch motion.

output torque with small volumes and mass while maintaining proper rated joint velocity.

The payload of the uterus manipulation is formed of the following several parts: 1) the weight of the uterus; 2) the deformation force of the vaginal tissue; 3) the adhesion between the uterus and other tissues in the abdominal cavity. Based on the suggestion from the local medical experts and the consideration of reserving additional load capacity, the rated load applied to the end-effector (see Fig. 5) of the robot is set as 50 N. Our robotic arm is used in the medical field, where the robot arm does not operate as fast as industrial robotic arms in terms of speed and acceleration. Therefore, when calculating the required output torque for each joint of the robot, we only consider the effects of the robot arm's self-weight and load and ignore the effects of inertial and Coriolis forces. To simplify the calculation, we mainly consider the extreme configuration of the robot arm, i.e., the robot is fully extended in a straight line, which is parallel to the ground. Of course, this extreme configuration does not occur in practice, but it can be used as an upper limit for joint torque selection. Since joints 2, 4, and 6 are more susceptible to gravity and load than joints 1, 3, 5, and 7, we calculate the torque required for these three joints. To simplify the design, actuator III was used for axes 1 and 2 of the robot, actuator II was used for axes 3 and 4, and actuator I was used for axes 5, 6 and 7. The simplified torque calculation equation is shown below:

$$T_i^d = \hat{W}_i \cdot \hat{l}_i + P^r \cdot \hat{L}_i \tag{1}$$

where T_i^d is the desired output torque of the joint i, $\hat{W}_i$ is the estimated wight of the rest of the robot connected to the output of joint i, $\hat{l}_i$ is the distance between the axis of joint i and the center of the mass, P^r is the rated payload applied at the end-effector which is set as 50 N as mentioned before, and $\hat{L}_i$ is the distance between the axis of joint i and end-effector. The estimated parameters and also the desired torque of the joints are shown in Table III. The torque required for each joint is smaller than the rated torque of our developed joints (see Table II and III), which means that the developed actuators can meet the payload requirements. The modified D-H parameters are used to model the kinematics of the robotic arm and the results are shown in the Table IV.

TABLE III
DESIRED TORQUE OF THE JOINT

Type	Joint 2	Joint 4	Joint 6
$\hat{W}_i$ (N)	100	50	20
$\hat{l}_i$ (m)	0.4	0.25	0.1
$\hat{L}_i$ (m)	0.8	0.5	0.2
T_i^d (Nm)	80	37.5	12

TABLE IV
MODIFIED D-H PARAMETERS OF THE ROBOT

i	1	2	3	4	5	6	7
α_{i-1} (rad)	0	$-\frac{\pi}{2}$	$\frac{\pi}{2}$	$-\frac{\pi}{2}$	$\frac{\pi}{2}$	$-\frac{\pi}{2}$	$-\frac{\pi}{2}$
a_{i-1} (mm)	0	0	0	0	0	0	93
d_i (mm)	194.9	0	298	0	267.4	0	0
θ_i (rad)	θ_1	θ_2	θ_3	θ_4	θ_5	$-\frac{\pi}{2}+\theta_6$	θ_7

C. Other Components

To facilitate preoperative positioning, the system is equipped with a 6-D force sensor that allows the assistant to quickly guide the robot to the desired position through admittance control (see Fig. 3(a)). A plastic handle with an integrated self-resetting switch is attached to the force sensor. The switch is pressed while the assistant holds the handle, thus the force sensor is activated. The primary surgeon uses a foot pedal interface (see Fig. 5(c)) to control the motion of the robot under the RCM constraint. In order of maneuvering frequency in each direction, the large pedal at the bottom controls the yaw motion of the RCM, the joystick at the top controls the

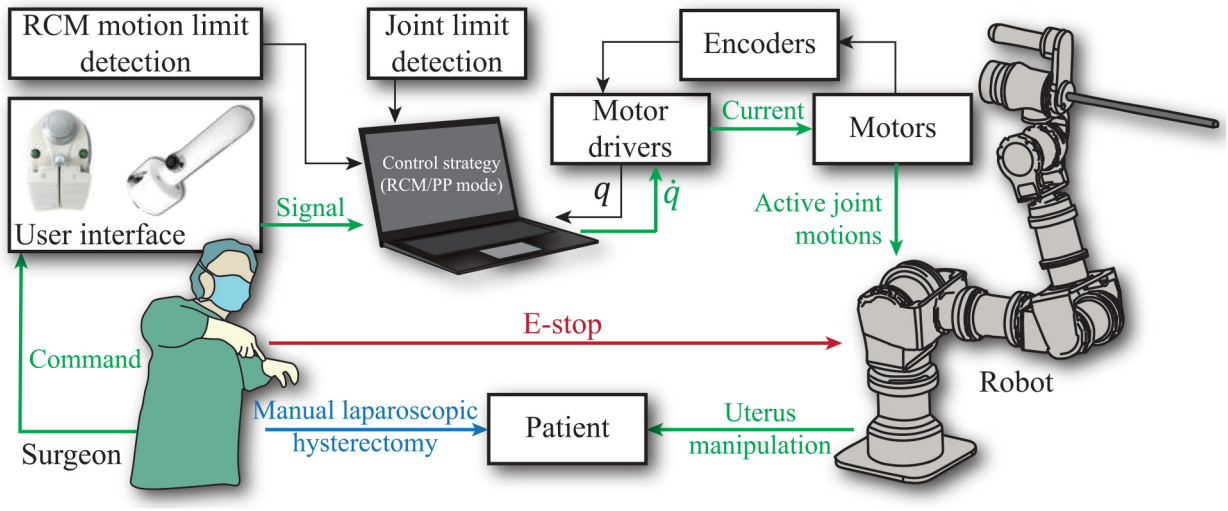

Fig. 6. The whole control architecture of the robot-assisted laparoscopic hysterectomy. (RCM: Remote center of motion; PP: Preoperational positioning.)

pitch motion, and the green button in the middle controls the roll motion.

The RUM uses the uterus manipulation rod as shown in Fig. 5(b), with various straight and curved (15°) tips. The manipulator is equipped with tips of different lengths to match different sizes of the uterus. A stopper on the posterior side of the tip is secured to the cervix to facilitate preoperative positioning and prevent the manipulator from poking the uterus. A quick pluggable mechanism is implemented on the manipulation rod to facilitate preoperational sterilization. As shown in Fig. 5(b), the cam handle rotates around the eccentric center to hold down the gripper. The deformation of the gripper can create enough friction to fix the rod in place.

IV. Control of the RUM

A. Control Architectures of the RUM

Fig. 6 demonstrates the complete control architecture of robot-assisted laparoscopic hysterectomy using the RUM. The architecture emphasizes a primary-surgeon-centered solution, where the surgeon can issue commands through the control interface to manipulate the RUM for uterus posture adjustment while performing routine bimanual uterus removal tasks. The robot is placed in a suitable position through a preoperative positioning (PP) control mode and locked with a manipulation rod inserted into the vaginal opening. The process is achieved by an assistant operating the robot using a force sensor control interface. A wired foot pedal control interface (modified from dental foot pedal) is provided to improve the robot's reliability in a noisy surgical environment and free the surgeon's hands. The primary surgeon controls the RUM via the foot pedal to move around the RCM point, i.e., the movement as shown in Fig. 6(c). In exceptional cases, such as when the foot pedal is not working, or other operations need to be performed with the foot, the surgeon can still order the assistant to manipulate the robot. In this operation, the assistant controls the robot via force sensors and manipulates the handle to move the rod around the RCM point. Both of these two operations are conducted under RCM mode, and all relevant algorithms will be described in the next section.

The Bechoff Industrial PC C6920 (Intel Core i5, Bechoff company, Germany) was used as the onboard PC to command the motor drivers as well as control the entire robot system. Gold Solo Twitter driver (10A/100V, 800 W, Elmo Motion Control, Israel) was selected for distributed controlling of seven modular actuators via the Ethercat communication protocol, which is a real-time, high-speed, and flexible industrial Ethernet for data communication in automation control systems, such as robotics systems [25]. The joint-level current, velocity and position limit of each motor is set in the motor driver. When the limit is reached, the robot is forced to stop, and the electromagnetic brake starts to operate. The RCM position limits of the robot are detected at the software level. The framework of the entire robot software control program is based on the Windows-based real-time system Twincat [26] and is programmed using the C and the PLC programming languages Structure Text (ST). The control frequency of the entire system is set to 1000 Hz. The foot pedal and force sensor signals are uploaded to Twincat via I/O and UDP communication protocols, respectively, and are integrated into the control loop as input values for the corresponding control strategy. The entire system uses 48V and 24V medical power supplies to support motors and other electronics (e.g., brakes, force sensors, foot pedals, etc.), respectively. An emergency stop button controlled by the surgeon, once activated, will lock all robot joints in place.

B. Control Strategies of the PP and RCM Mode

For robot-enabled uterus manipulation, the robot is firstly controlled in the preoperational positioning (PP) mode for localizing itself towards the vaginal opening (see Fig. 7(a)). The preoperational positioning is realized by the force sensor installed on the robot. Firstly, the force measured by the sensor

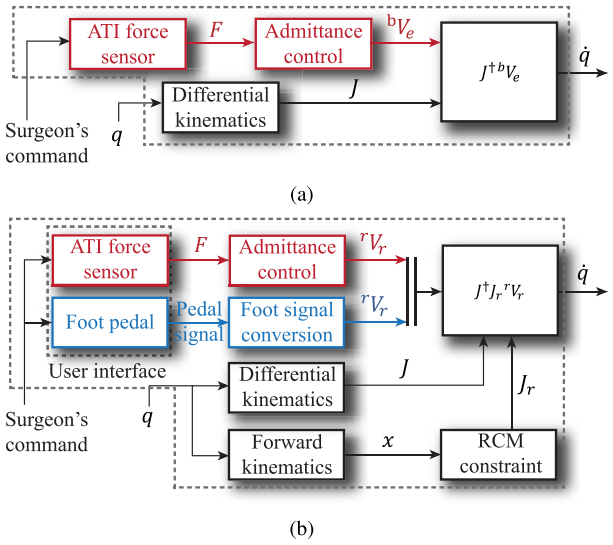

Fig. 7. The control strategies. (a) The preoperational positioning (PP) control mode for the RUM. (b) The RCM control mode for the RUM.

will be converted into a force applied on the end-effector,

$$^e\boldsymbol{F}_e = \begin{bmatrix} {}^e_s\boldsymbol{R} & \boldsymbol{0}_{3\times3} \\ [{}^e\boldsymbol{P}_{sorg}]_\times \cdot {}^e_s\boldsymbol{R} & {}^e_s\boldsymbol{R} \end{bmatrix} \cdot {}^s\boldsymbol{F}_s \tag{2}$$

where $^s\boldsymbol{F}_s = \begin{bmatrix} {}^sf_s^T & {}^s\boldsymbol{\tau}_s^T \end{bmatrix}^T \in \mathbb{R}^{6\times1}$ is the force applied on the force sensor expressed in the sensor frame {s}, $^e\boldsymbol{F}_e = \begin{bmatrix} {}^ef_e^T & {}^e\boldsymbol{\tau}_e^T \end{bmatrix}^T \in \mathbb{R}^{6\times1}$ is the converted force applied on the end-effector expressed in the end-effector frame {e}, ${}^e_s\boldsymbol{R} \in \mathbb{R}^{3\times3}$ and $^e\boldsymbol{P}_{sorg} \in \mathbb{R}^{3\times1}$ are the rotation matrix and translation vector from the sensor frame {s} to the end-effector frame {e}, and the $[{}^e\boldsymbol{P}_{sorg}]_\times$ is the skew-symmetric matrix associated with the vector $^e\boldsymbol{P}_{sorg}$. Then a mapping function is adopted to convert the force $^e\boldsymbol{F}_e$ into the velocity $^e\boldsymbol{V}_e$,

$$^e\boldsymbol{V}_e{}^{(i)} = \mathcal{M}\left({}^e\boldsymbol{F}_e^{(i)}\right) \tag{3}$$

where $^e\boldsymbol{V}_e \in \mathbb{R}^{6\times1}$ is the desired velocity of the end-effector expressed in the end-effector frame {e}, $^e\boldsymbol{V}_e{}^{(i)}$ is the i_{th} component of the vector $^e\boldsymbol{V}_e$, $^e\boldsymbol{F}_e{}^{(i)}$ is the i_{th} component of the vector $^e\boldsymbol{F}_e$, and the mapping function $v = \mathcal{M}(f)$ is formed as

$$v = \begin{cases} \text{sign}(f) \cdot k_1 \cdot \sin(k_2 \cdot \delta f), & 0 \le \delta f < \widehat{\delta f} \\ \text{sign}(f) \cdot \widehat{\delta f}, & \delta f \ge \widehat{\delta f} \end{cases} \tag{4}$$

$$\delta f = \begin{cases} |f| - \widehat{f}, & |f| > \widehat{f}, \\ 0, & |f| \le \widehat{f} \end{cases} \tag{5}$$

where k_1 and k_2 are the coefficients of the mapping function which are set as $\pi/(2\widehat{f})$ and $\widehat{f}$ to form a smooth S-shaped mapping function, δf occurs only when the applied force is larger than the predetermined threshold $\widehat{f}$, and $\widehat{\delta f}$ is the maximum value of δf over which the velocity will be a constant value. With the velocity $^e\boldsymbol{V}_e{}^{(i)}$, we can calculate the joint velocity which will be sent to the motor driver,

$$\dot{\boldsymbol{q}} = J^\dagger(\boldsymbol{q}) \cdot {}^b\boldsymbol{V}_e = J^\dagger(\boldsymbol{q}) \cdot \begin{bmatrix} {}^b_e\boldsymbol{R} & \boldsymbol{0}_{3\times3} \\ \boldsymbol{0}_{3\times3} & {}^b_e\boldsymbol{R} \end{bmatrix} \cdot {}^e\boldsymbol{V}_e \tag{6}$$

where $\boldsymbol{q} \in \mathbb{R}^{7\times1}$ is the joint position, $\dot{\boldsymbol{q}} \in \mathbb{R}^{7\times1}$ is the joint velocity, $^b\boldsymbol{V}_e$ is the desired velocity of the end-effector expressed in the robot base frame {b}, ${}^b_e\boldsymbol{R} \in \mathbb{R}^{3\times3}$ is the rotation matrix from the end-effector frame {e} to the base frame {b}, and $J^\dagger(\boldsymbol{q}) = J(\boldsymbol{q})^T \cdot (J(\boldsymbol{q}) \cdot J(\boldsymbol{q})^T)^{-1} \in \mathbb{R}^{7\times6}$ is the right pseudo inverse of the geometric jacobian $J(\boldsymbol{q})$ mapping the joint velocity to the end-effector velocity.

As soon as the preoperational positioning is finished and the manipulation rod is inserted into the uterus through the vaginal opening, the RCM mode (see Fig. 7(b)) is enabled. In the RCM mode, the rod is only allowed to rotate around the cervix. Thus the velocity of the RCM point of the rod expressed in the RCM frame {r} is as follows,

$$^r\boldsymbol{V}_r = \begin{bmatrix} 0 & 0 & 0 & w_x & w_y & w_z \end{bmatrix}^T \tag{7}$$

In this case, the manipulation rod has no lateral velocity due to the RCM constraint. The axial velocity of the rod is also eliminated to avoid excessive movement of the rod in the axial direction that may lead to stabbing the uterus during operation. The insertion depth of the rod is determined at the preoperational positioning.

We have two interfaces. i.e., the foot-pedal interface and the force sensor interface, to generate the RCM velocity $^r\boldsymbol{V}_r$. Pitch, yaw and roll button of the pedal (see Fig. 5(b)) are associated with the angular velocities w_x, w_y and w_z, respectively. A constant angular velocity occurs once the corresponding button is activated. In case the force sensor is used for the RCM mode, $^s\boldsymbol{F}_s$ is converted into a force applied on the RCM point,

$$^r\boldsymbol{F}_r = \begin{bmatrix} \boldsymbol{0}_{3\times3} & \boldsymbol{0}_{3\times3} \\ \boldsymbol{0}_{3\times3} & \boldsymbol{I}_{3\times3} \end{bmatrix} \cdot \begin{bmatrix} {}^r_s\boldsymbol{R} & \boldsymbol{0}_{3\times3} \\ [{}^r\boldsymbol{P}_{sorg}]_\times \cdot {}^r_s\boldsymbol{R} & {}^r_s\boldsymbol{R} \end{bmatrix} \cdot {}^s\boldsymbol{F}_s \tag{8}$$

where $^r\boldsymbol{F}_r = \begin{bmatrix} 0 & 0 & 0 & \tau_x & \tau_y & \tau_z \end{bmatrix}^T \in \mathbb{R}^{6\times1}$ is the force applied on the RCM point expressed in the RCM frame {r}, ${}^r_s\boldsymbol{R} \in \mathbb{R}^{3\times3}$ and $^r\boldsymbol{P}_{sorg} \in \mathbb{R}^{3\times1}$ is the rotation matrix and translation vector from the sensor frame {s} to the RCM frame {r}, and the $[{}^r\boldsymbol{P}_{sorg}]_\times$ is the skew-symmetric matrix associated with the vector $^r\boldsymbol{P}_{sorg}$. The torques τ_x, τ_y and τ_z are mapped to generate the constant angular velocities w_x, w_y and w_z.

There is a positional error between the actual robot's RCM point and the desired point due to deviations in the robot's motion or changes in the patient's position. We introduce this error as feedback to generate the linear velocity of the robot on the RCM frame to reduce the error,

$$\begin{bmatrix} v_x & v_y & v_z \end{bmatrix}^T = \boldsymbol{K_e} \cdot \begin{bmatrix} x_e & y_e & z_e \end{bmatrix}^T \tag{9}$$

where x_e, y_e and z_e are the linear velocities of the robot along the x, y, z axes of the RCM frame, respectively. $\boldsymbol{K_e} \in \mathbb{R}^{3\times3}$ is the gain diagonal matrix that maps the errors to the velocities. x_e, y_e and z_e are the position errors between the actual RCM point and the desired RCM point as shown in the RCM frame. The velocity $^r\boldsymbol{V_r}$ is reformulated as $\begin{bmatrix} v_x & v_y & v_z & w_x & w_y & w_z \end{bmatrix}^T$, which is then converted to the velocity of the end-effector expressed in the robot base frame by left multiplying the RCM jacobian $\boldsymbol{J_r(q)}$,

$$^b\boldsymbol{V}_e = \underbrace{\begin{bmatrix} {}^b_e\boldsymbol{R} & \boldsymbol{0}_{3\times3} \\ \boldsymbol{0}_{3\times3} & {}^b_e\boldsymbol{R} \end{bmatrix} \cdot \begin{bmatrix} {}^e_r\boldsymbol{R} & -{}^e_r\boldsymbol{R} \cdot [{}^r\boldsymbol{P}_{eorg}]_\times \\ \boldsymbol{0}_{3\times3} & {}^e_r\boldsymbol{R} \end{bmatrix}}_{\boldsymbol{J_r(q)}} \cdot {}^r\boldsymbol{V}_r \tag{10}$$

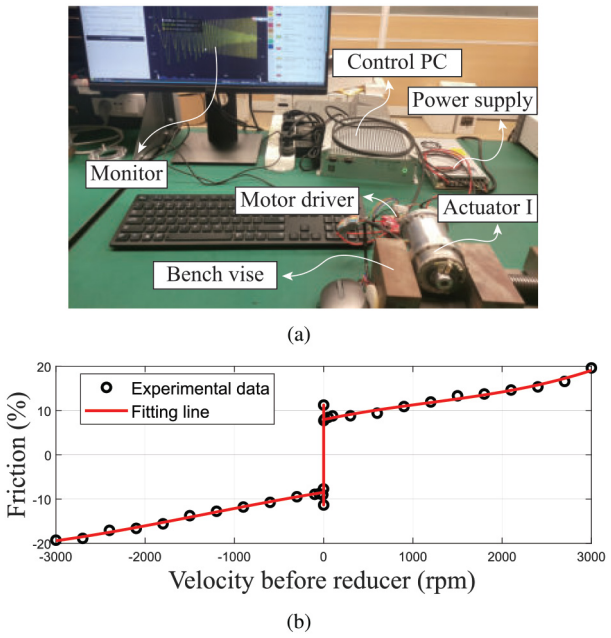

Fig. 8. The friction test of the modular actuator. (a) Experimental setup for friction test. (b) The velocity-friction result.

where ${}^{e}_{r}\boldsymbol{R} \in \mathbb{R}^{3\times3}$ and ${}^{e}\boldsymbol{P}_{rorg} \in \mathbb{R}^{3\times1}$ is the rotation matrix and translation vector from the sensor frame {r} to the end-effector frame {e}. The joint velocity $\dot{\boldsymbol{q}}$ sent to the motor driver is then calculated by using (6).

V. Experiments and Results

In this section, we performed experiments to measure the friction of the modular actuator, repeatability of RCM constraints and assess the robot's feasibility in simulated laparoscopic hysterectomy.

A. Friction Test of the Modular Actuator

As shown in Table II, the basic performance of the modular actuator, such as rated output torque and rated output speed, is determined by the selected motor and harmonic driver. In addition to this, the performance of the actuator is also influenced by the friction. Excessive friction can lead to low available output torque and severe heat generation. The friction force is influenced by the quality of bearings and harmonic reducer of the actuator, as well as the quality of machining and mounting process of the relevant components, and varies with velocity, temperature and external load [27].

Therefore measuring the friction of our modular actuators helps to analyze their performance. The experimental setup is shown in Fig. 8(a), the modular actuator is held by a bench vise and commanded by the motor driver to move at a constant velocity. The value of the current is recorded and converted into a torque value, which is the friction when the actuator is not subjected to an external load. The friction data at several motor velocities ranging from -3000 rpm to $+3000$ rpm was collected. It is worth noting that the actuator is affected by static friction during start-up. Therefore, we also tested the minimum torques that would drive the actuator in forward and reverse rotation and considered them to be the static friction torques. Take the Actuator I as an example, Fig. 8(b) shows the result of the friction test. The black dots indicate the experimentally recorded data, and the red line indicates the multi-segment polynomial curves used to fit the data points. Friction is expressed in the ratio of the rated output torque. The friction is about 10 percent of the rated torque at the velocity of 1000 rpm and less than 20 percent at 3000 rpm. These frictions are less than the joint friction of commercial collaborative robot arms discussed in [27]. It can be seen that the transmission efficiency of the modular actuator is between 80 percent and 90 percent. Since there are no modular actuators on the market with marked transmission efficiency, we compare our actuator with a Maxon motor with approximate output torque and reduction ratio (brushless motor EC 60 flat ϕ60 mm + planetary gearbox GP 52 C ϕ52 mm). The transmission efficiency of this motor and planetary gear is only 85 percent and 75 percent, respectively, and the overall transmission efficiency is 64 percent, which is much lower than the transmission efficiency of our modular actuator. Therefore, we think the friction of our modular actuator is acceptable equipped with a brake and harmonic reducer.

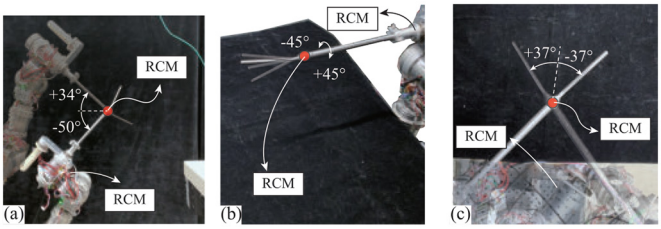

Fig. 9. Motion of the RUM under the RCM constraint. (a) Pitch motion; (b) Roll motion; (c) Yaw motion.

B. RCM Repeatability Verification Experiment

The previous section shows that the RUM is controlled algorithmically to have the RCM constraints.

As shown in Fig. 9, the RUM can achieve the required pitch motion range (i.e., $-50° \sim 34°$) and yaw motion range ($\pm37°$). It should be noted that the roll motion is achieved directly by the last joint of the RUM and can rotate infinitely. However, considering the actual situation, the roll motion is limited to a defined range of angles ($\pm45°$).

In this experiment, we evaluate the repeatability of the RCM constraint when the robot is moving in RCM mode. Optical tracking is a 3D positioning technique based on multiple cameras equipped with infrared (IR) filters and IR LEDs, monitoring a defined measurement space in which the exact position of the infrared reflective markers can be obtained. As shown in Fig. 10(a), a frame with integrated four infrared reflective markers is fixed to the end of the robot. We use OptiTrack's optical tracking technology to obtain the positions of the four markers on the frame and solve for the RCM points through geometric relationships. The cameras used are Prime^{X} 13, and the software is the Motive 2.0 motion tracking software.

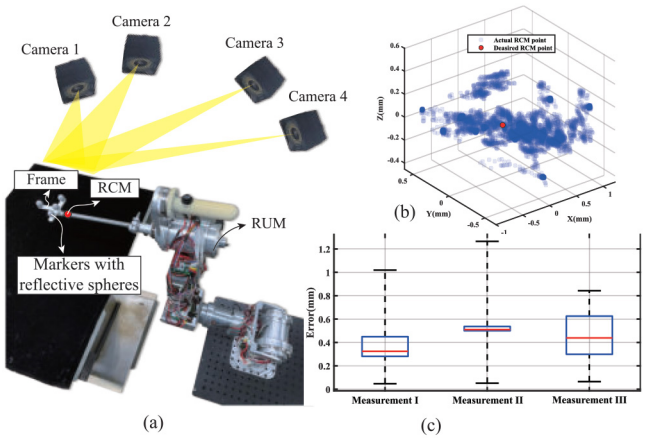

Fig. 10. (a) The experimental setup of the measurement of the RCM repeatability. A support frame is mounted on the end of the RUM with four integrated infrared reflective markers; (b) Repeatability of the RCM points. The red node represents the desired RCM point, and the translucent blue nodes represent the actual RCM points observed by the optical tracking system; (c) Errors between each actual RCM point and the desired RCM point of each measurement set as shown in the boxplot.

During the measurement, the robot was controlled by the foot pedal to move under the RCM constraint within the required motion range, and three sets of measurements were conducted. Fig. 10(b) presents the measured actual RCM points of the combining three measurements, which are noted by the translucent blue nodes. The red node represents the desired RCM point defined by the RCM point at the robot's initial configuration. All the nodes are shown in the frame of the tracking system. Fig. 10(c) shows the displacement errors between the actual RCM points and the desired point of each set represented as the boxplot. It can be observed that the maximum errors of the set I, II and III are 1.02 mm, 1.26 mm, and 0.84 mm, respectively. The mean absolute errors (MAE) of each measurement are 0.41 mm, 0.55mm, and 0.44 mm, respectively. The overall MAE between the actual RCM points and the desired RCM point is 0.49 mm. These errors consist of errors in the kinematic parameters of the robot, the RCM motion algorithm, and the measurement system itself. Generally speaking, the above errors are acceptable for the uterus manipulation task.

C. Study of the Simulated Robot-Assisted Laparoscopic Hysterectomy

To further verify the feasibility of the proposed robot-enabled uterus manipulator, a simulated study of the robotic laparoscopic hysterectomy was performed using the adult manikin models. Staff with engineering and surgical backgrounds participated in this study and experienced all operations.

The preoperational setup of the surgery is shown in Fig. 11, which could be clarified as the following sub-procedures.

(1) Keeping the robot in a suitable initial position (see Fig. 3(a)), it is then moved between the patient's legs by means of a passive movement base. The robot is positioned roughly symmetrically between the legs and its end-effector is roughly 25 cm away from the vaginal opening (see figure: reffig:preoperation(a)).
(2) Next, the manipulation rod is inserted through the vagina into the uterus, whose insertion depth is adjusted so that the stopper is placed at the cervix and the instrument tip is inside the uterus (see Fig. 11(a)). For this step, various instrument tips with different lengths can be selected for proper tensioning of the uterus.
(3) The assistant then uses a handle with an integrated force sensor to drag the robot arm close to the manipulation rod through the admittance control and connects the rod to the robot arm through a quick-pluggable mechanism (see Fig. 11(b) and (c)).
(4) Finally, the assistant checks whether the robotic arm and the manipulation rod are in the proper position. Preoperative positioning is completed.

Once the preoperative positioning is completed, the prime surgeon and the assistant can control the robot under RCM constraints via the foot pedal and the force sensor handle. Fig. 12(a) shows the robot controlled by the user through the foot pedal, while Fig. 12(b)-(d) show the robot located in the initial pose, prying the uterus upwards and swinging the uterus to the right, respectively. Fig. 12(e)-(f), on the other hand, show the user controlling the robot by force sensors to twist the uterus, manipulate it upward and rightward, respectively.

Staff with surgical, especially hysterectomy background, was invited to use the RUM, including all the procedures (preoperative positioning, controlling using foot pedal and force sensor) and gave the feedback. Similar in size and shape to a human arm, the RUM is compact and slender and can easily be placed in the narrow space between the patient's legs. Compared with adjustment by passive x-y-z platform, positioning of the robot by admittance control is more intuitive and convenient, which is potential to reduce the preoperative setup time for clinical procedures. The RCM constrains the robot to avoid compression of the bony structures by the manipulation rod during the operation. During manual manipulation of the uterus, the assistant may unconsciously push the rod forward while lifting the uterus upward thus potentially puncturing the uterus, which does not occur during RCM-constrained robotic manipulation.

There are also some defects of the RUM, such as the small size of the foot pedal and the large number of buttons, which affect the surgeon's operating experience. The assistant has to keep pressing the circular button on the force sensor handle when manipulating the robotic using admittance control, which also affects the operating experience. The ergonomics and human-machine interaction experience should be improved in the clinical version.

Three subjects were invited to manually simulate uterus manipulation without the use of the robotic system. Fig. 13(a) shows the experimental for this study. Subjects used a manipulation rod to pass through the simulated plastic cervix and track the desired trajectory on the 3D print part (the blue curve). The trajectory is the outer contour formed by the pitch motion from -30 degrees to $+30$ degrees and the yaw motion from -30 degrees to $+30$ degrees. A marker with the reflective sphere was mounted at the top of the manipulation rod,

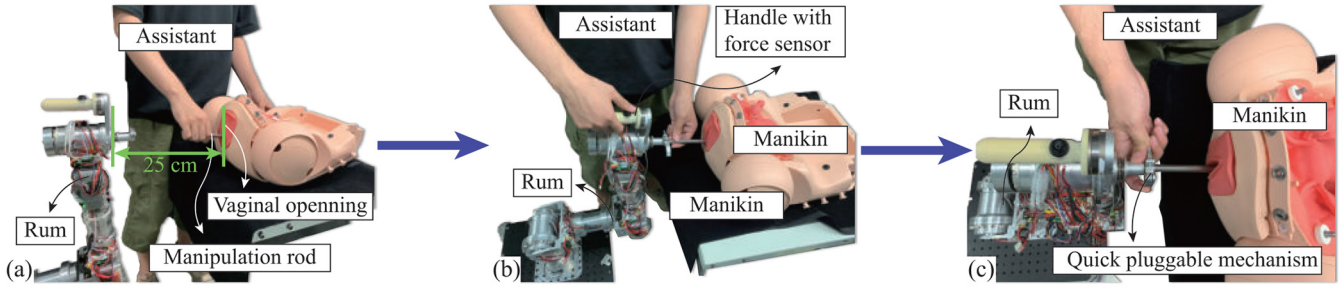

Fig. 11. Preoperative setup of the RUM during laparoscopic hysterectomy. (a) Placement of the robotic arm and insertion of the manipulation rod into the uterus through the vagina. (b) Guidance of the robotic arm approaching the placed manipulation rod by admittance control. (c) Connection of the robot and the rod through the quick pluggable mechanism.

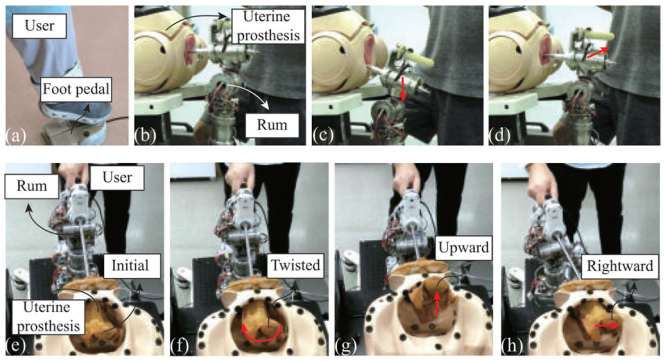

Fig. 12. The manipulation of the uterus under RCM motion. (a) Foot pedal control interface; (b)-(d) Various configurations of the robot; (e)-(h) Various configurations of the uterus under the manipulation of the robot via the admittance control.

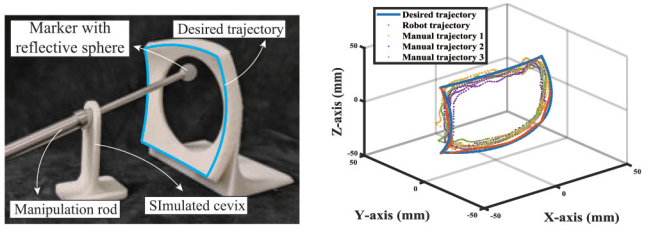

Fig. 13. (a) The experimental setup of the trajectory tracking experiment. (b) The results of the robotic trajectory tracking and manual trajectory tracking.

the actual trajectory thereby can be recorded using the optical tracking system mentioned before. The trajectory tracking results of the subject were recorded and compared with the results of the simulated uterus manipulation using the robot. Fig. 13(b) shows the results of the experiment. It can be noticed that the trajectory tracked using the robot is smoother and has less deviation from the desired trajectory, while the trajectory tracked by the three subjects is more jerky and has more deviation from the desired trajectory. Thus, the use of a robotic system can improve the manipulation accuracy. It can be expected that robotic uterus manipulation thus causes less invasive to the patient.

VI. Conclusion and Future Work

The RUM was designed and developed in this work, mainly comprising a 7 DoF robotic arm dedicated to the uterus manipulation task during laparoscopic hysterectomy and a passive mobile base for positioning. The robotic arm consists of modular actuator of three rated output torque (27, 50, and 100 Nm), which can withstand a minimum of 50 N payload at the end-effector. The entire system can control the manipulation rod to rotate around the RCM point by software. The available RCM motion ranges are: 1) pitch motion from $-50° \sim 34°$; 2) yaw motion from $-37° \sim 37°$; 3) and the constrained roll motion from $-45° \sim 45°$. Two interfaces, i.e., foot pedal and force sensor, are provided for controlling the robot in the preoperational positioning mode and the RCM mode. The friction of the modular actuator is acceptable. The overall mean absolute error between the actual RCM points and the desired RCM point is 0.49 mm, which is acceptable for the uterus manipulation task. Based on the feedback from the staff with surgical backgrounds, the robot is suitable for placement in the narrow space between the patient's legs due to its compact and slender structure. Dragging the robot via admittance control is intuitive and convenient, with which can save preoperative positioning time. The RCM constraints of the robot reduce the risk of the rod colliding with the bony structures of the patient and the risk of the rod piercing the uterus. Ergonomic and human-machine interaction should be improved.

We plan to improve the industrial design, cable management, mechanical design of the RUM, and ergonomics in the future. The animal test, cadaver test, and even the clinical trial are also considered for the next version of the robot. The sterilization of instruments and the isolation of the robot body from the sterile surgical environment should be considered more rigorously.

References

[1] M. K. Whiteman *et al.*, "Inpatient hysterectomy surveillance in the United States, 2000–2004," *Amer. J. Obstetrics Gynecol.*, vol. 198, no. 1, pp. 34–37, 2008.
[2] H. Reich, J. DeCaprio, and F. McGlynn, "Laparoscopic hysterectomy," *J. Gynecol. Surg.*, vol. 5, no. 2, pp. 213–216, 1989.
[3] M. Sculpher, A. Manca, J. Abbott, J. Fountain, S. Mason, and R. Garry, "Cost effectiveness analysis of laparoscopic hysterectomy compared with standard hysterectomy: Results from a randomised trial," *Brit. Med. J.*, vol. 328, no. 7432, p. 134, 2004.
[4] K. Swan, J. Kim, and A. P. Advincula, "Advanced uterine manipulation technologies," *Surg. Technol. Int.*, vol. 20, pp. 215–220, Oct. 2010.

[5] M. A. Martínez-Maestre, P. Gambadauro, C. González-Cejudo, and R. Torrejón, "Total laparoscopic hysterectomy with and without robotic assistance: A prospective controlled study," *Surg. Innov.*, vol. 21, no. 3, pp. 250–255, 2014.
[6] A. G. Visco and A. P. Advincula, "Robotic gynecologic surgery," *Obstetrics Gynecol.*, vol. 112, no. 6, pp. 1369–1384, 2008.
[7] W. Von Pechmann, S. C. Yoon, B. Lane, K. Lipford, and A. Cox, "Table-mounted surgical instrument stabilizers with single-handed or voice activated maneuverability," U.S. Patent Appl. 12 584 366, Jun./Jul. 2010.
[8] J. S. Singh and J. Singh, "Repositionable medical instrument support systems, devices, and methods," U.S. Patent 9 532 837, Jan.–Mar. 2017.
[9] R. H. Taylor, "A perspective on medical robotics," *Proc. IEEE*, vol. 94, no. 9, pp. 1652–1664, Sep. 2006.
[10] N. Akrivos and P. Barton-Smith, "A pilot study of robotic uterine and vaginal vault manipulation: The ViKY uterine positioner^{TM}," *J. Robot. Surg.*, vol. 7, no. 4, pp. 371–375, 2013.
[11] J.-A. Long *et al.*, "Development of miniaturized light endoscope-holder robot for laparoscopic surgery," *J. Endourol.*, vol. 21, no. 8, pp. 911–914, 2007.
[12] S. Voros, G.-P. Haber, J.-F. Menudet, J.-A. Long, and P. Cinquin, "ViKY robotic scope holder: Initial clinical experience and preliminary results using instrument tracking," *IEEE/ASME Trans. Mechatronics*, vol. 15, no. 6, pp. 879–886, Dec. 2010.
[13] H. M. Yip, P. Li, D. Navarro-Alarcon, and Y.-H. Liu, "Towards developing a robot assistant for uterus positioning during hysterectomy: System design and experiments," *Robot. Biomimetics*, vol. 1, no. 1, pp. 1–11, 2014.
[14] H. M. Yip *et al.*, "A collaborative robotic uterine positioning system for laparoscopic hysterectomy: Design and experiments," *Int. J. Med. Robot. Comput. Assist. Surg.*, vol. 16, no. 4, p. e2103, 2020.
[15] C.-H. Kuo, J. S. Dai, and P. Dasgupta, "Kinematic design considerations for minimally invasive surgical robots: An overview," *Int. J. Med. Robot. Comput. Assist. Surg.*, vol. 8, no. 2, pp. 127–145, 2012.
[16] J. Wu *et al.*, "An optimized tilt mechanism for a new steady-hand eye robot," in *Proc. IEEE/RSJ Int. Conf. Intell. Robots Syst. (IROS)*, 2020, pp. 3105–3111.
[17] U. Hagn, "The aspect of versatility in the design of a lightweight robot for surgical applications," Ph.D. dissertation, Dept. Mech. Eng., Univ. Hannover, Hanover, Germany, 2011.
[18] E. Dombre *et al.*, "MARGE project: Design, modeling and control of assistive devices for minimally invasive surgery," in *Proc. Int. Conf. Med. Image Comput. Comput. Assist. Interv.*, 2004, pp. 1–8.
[19] B. Yang *et al.*, "Adaptive FOV control of laparoscopes with programmable composed constraints," *IEEE Trans. Med. Robot. Bionics*, vol. 1, no. 4, pp. 206–217, Nov. 2019.
[20] J. Sandoval, G. Poisson, and P. Vieyres, "A new kinematic formulation of the RCM constraint for redundant torque-controlled robots," in *Proc. IEEE/RSJ Int. Conf. Intell. Robots Syst. (IROS)*, 2017, pp. 4576–4581.
[21] H. Su, G. Ferrigno, and E. De Momi, "Adaptive decoupling control of a serial redundant robot for teleoperated minimally invasive surgery," in *Proc. IEEE ICRA Workshop Supervised Auton. Surg. Robot.*, 2018, pp. 1–6.
[22] B. Siciliano, "Kinematic control of redundant robot manipulators: A tutorial," *J. Intell. Robot. Syst.*, vol. 3, no. 3, pp. 201–212, 1990.
[23] B. Rocco, A. Lorusso, R. Coelho, K. Palmer, and V. Patel, "Building a robotic program," *Scand. J. Surg.*, vol. 98, no. 2, pp. 72–75, 2009.
[24] J. P. Ruurda, P. L. Visser, and I. A. M. J. Broeders, "Analysis of procedure time in robot-assisted surgery: Comparative study in laparoscopic cholecystectomy," *Comput.-Aided Surg.*, vol. 8, no. 1, pp. 24–29, 2003.
[25] D. Jansen and H. Buttner, "Real-time Ethernet: The EtherCAT solution," *Comput. Control Eng.*, vol. 15, no. 1, pp. 16–21, 2004.
[26] S. M. Blair, *Beckhoff and TwinCAT 3 System Development Guide*, Univ. Strathclyde, Glasgow, Scotland, 2015.
[27] L. Gao, J. Yuan, Z. Han, S. Wang, and N. Wang, "A friction model with velocity, temperature and load torque effects for collaborative industrial robot joints," in *Proc. IEEE/RSJ Int. Conf. Intell. Robots Syst. (IROS)*. 2017, pp. 3027–3032.